Received: 25 October 2022 | Revised: 8 December 2022 | Accepted: 12 December 2022

IET Nanodielectrics

DOI: 10.1049/nde2.12040

ORIGINAL RESEARCH

Resilient electret film-based vibrational energy harvesters with a V-shaped counter electrode

Xiaoya Yang[1] | Xingchen Ma[1,2] | Chuan Ding[1] | Gerhard M. Sessler[3] | Heinz von Seggern[4] | Mario Kupnik[3] | Ying Dai[1] | Pengfei He[1] | Xiaoqing Zhang[2]

[1]School of Aerospace Engineering and Applied Mechanics, Tongji University, Shanghai, China

[2]Shanghai Key Laboratory of Special Artificial Microstructure Materials and Technology, School of Physics Science and Engineering, Tongji University, Shanghai, China

[3]Department of Electrical Engineering and Information Technology, Technische Universität Darmstadt, Darmstadt, Germany

[4]Department of Materials and Earth Sciences, Technische Universität Darmstadt, Darmstadt, Germany

Correspondence

Ying Dai and Pengfei He, School of Aerospace Engineering and Applied Mechanics, Tongji University, Shanghai, 200092, China.
Email: ydai@tongji.edu.cn and ph232@tongji.edu.cn

Xiaoqing Zhang, Shanghai Key Laboratory of Special Artificial Microstructure Materials and Technology, School of Physics Science and Engineering, Tongji University, Shanghai, China.
Email: x.zhang@tongji.edu.cn

Funding information

National Natural Science Foundation of China, Grant/Award Numbers: 61761136004, 62201392; Shanghai Post-doctoral Excellence Program, Grant/Award Number: 2021341; Deutsche Forschungsgemeinschaft, Grant/Award Numbers: KU 3498/1-1, SE 941/19-1, SE 941/21-1

Abstract

Vibrational energy harvesters, which can convert mechanical energy distributed widely in the surrounding environment to electrical energy in a convenient, eco-friendly and sustainable way, have attracted great attention in both academia and industry. In this study, a resilient electret film-based vibrational energy harvester with a V-shaped counter electrode is introduced, simulated and constructed. A negatively charged fluorinated polyethylene propylene (FEP) electret film with a wavy shape was adopted in the devices, achieving simultaneously a stable embedded biased voltage and a large tensile deformation during vibration. The influences of the factors on the performance of the device, including the initial stretching state of the resilient electret film, seismic mass and depth of the V-shape counter electrode, were analyzed comprehensively with finite element simulation and compared to experiments. Further, the structure of the device was optimised for generating a high output power, and a good agreement between the simulation and experimental data was achieved. Additionally, the resonant frequency of the device can be easily tuned between 28 and 68 Hz by merely adjusting the initial stretching state of the wavy FEP electret film, guaranteeing great superiority for broad bandwidth energy harvesting applications. For an optimised energy harvester with a volume of only $15 \times 5 \times 1.7$ mm^3 and a tiny seismic mass of 25 mg, and a normalized output power referring to $1 \times g$ (g is the gravity of the Earth) up to 547 μW was obtained at its resonant frequency of 28 Hz. These results demonstrate that such a miniaturised vibrational energy harvester is a promising electrical energy supplier for low-power-consumption electronic devices, in particular in wireless sensor networks.

KEYWORDS

resilient electret film, tunable resonant frequency, V-shaped counter electrode, vibrational energy harvesting

1 | INTRODUCTION

Vibrational energy is one of the ubiquitous and easily harvested mechanical energy sources in the environment [1–6]. Various electromagnetic, piezoelectric and electrostatic energy harvesters have been designed [7–10] to provide sustainable energy for low-power electronic devices [11–13] by converting mechanical vibrational energy into electrical energy [14–16], enabling convenient self-powered automation functions.

Xiaoya Yang and Xingchen Ma authors contributed equally.

Generally, an electrostatic vibrational energy harvester utilizes a variable capacitor as the transduction element which is either charged by an external bias voltage or embedded with electrets [17–20]. For the homocharge electret polymer films which are often utilized in electrostatic energy harvesters, the typical value of the effective surface charge density ranges from 0.1 to 1 mC/m^2. The electrostatic energy harvesters embedded with electrets have captured much attention given their features such as self-powered capability (no bias voltage required), compatibility with MEMS processes, high conversion efficiency, simple implementation and eco-friendliness [21–28].

There exist two main factors that influence the performance of the electret-based electrostatic energy harvester. One is the electret property of the functional polymers, and the other is the mechanical structure of the device. In this study, a vibrational energy harvester, consisting of a highly resilient fluorinated polyethylene propylene (FEP) electret film with a wavy shape, a V-shaped counter and a small seismic mass was designed, simulated and fabricated. A finite element (FE) simulation model for the energy harvester was established and validated by the experiments first and then it was used to optimize the performance of the device. The influence of the initial state of components and some variable structural parameters on the resonant frequency and output power of the device has been investigated systematically.

2 | STRUCTURE AND WORKING PRINCIPLE OF THE ENERGY HARVESTER

The geometric and material parameters of the electrostatic vibrational energy harvester based on the negatively charged FEP electret film (Figure 1) are listed in Table 1. The FEP electret film used here has a wave-shaped structure which makes it very resilient [29–31]. The surface charge density on one side of the FEP film was around 0.42 mC/m^2, and the other side of the film was metalised with 100-nm-thick Al. The negatively charged FEP films were chosen in this study since the negative charges are significantly more stable than positive charges in FEP [32]. In order to improve the performance of the device, a V-shaped counter electrode was designed (Figure 1), considering the fact that such a structure can enlarge the variation of the device capacitance during vibration. The V-shaped counter electrode serves as a support frame to fix the two ends of the FEP electret film as well. A seismic mass was cemented in the center of the FEP film to provide an inertial force during vibration.

In order to assess the performance of the fabricated energy harvester, its bottom is fixed on a shaker, which exerts a vertical cosine acceleration excitation to the device. During the vibration process, the resilient wave-shaped FEP electret film is stretched, leading to the change of air gap thickness between the electret film and the bottom electrode, and, thus, a reorganization of the induced charge on both electrodes in short circuits or a variation of voltage between the two electrodes in open circuits will be detected. When a load resistor is connected between the two electrodes, the current flows through it, and, thus, the vibrational energy is converted into electrical energy.

The working principle of the electret-based electrostatic energy harvester is schematically illustrated in Figures 2a–c where a variable capacitor model was used and simplified as a parallel plate capacitor. Assuming the electret film has a uniform surface charge density, the distributions of induced charge on the two electrodes are also uniform. According to Gauss' theorem and Kirchhoff's second law in short circuits,

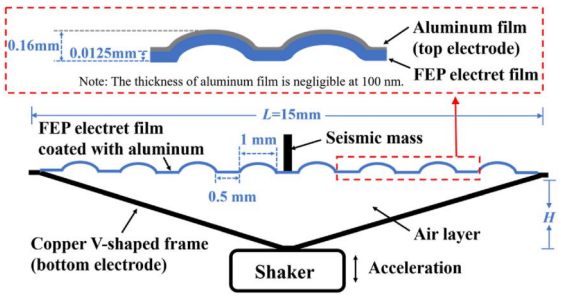

FIGURE 1 Schematic diagram of the resilient wavy electret film-based vibrational energy harvester with a V-shaped counter electrode.

TABLE 1 Geometric and material parameters of the vibrational energy harvester

Component (Material)	Parameters	Values
FEP electret film	Initial effective length L	15 mm
	Width W	5 mm
	Thickness d	12.5 μm
	Height of ripple t_{max}	160 μm
	Length of ripple l_1	1 mm
	Length between ripples l_2	0.5 mm
	Density ρ	2.15 × 10^3 kg/m^3
	Young's modulus E	460 MPa
	Poisson's ratio ν	0.3
	Surface charge density σ	0.42 mC/m^2
	Relative permittivity ε_r	2.1
Seismic mass (Cu)	Width	5 mm
	Density	8.8 × 10^3 kg/m^3
	Weight m_s	0.025–0.1 g
Top electrode (Al)	Thickness	100 nm
V-shaped counter electrode (Cu)	Horizontal length	15 mm
	Maximum depth H	2 mm
	Width	5 mm
	Young's modulus	108 GPa
	Poisson's ratio	0.35

the relationship between the electric field of the air gap and the electret layer can be expressed as follows [33].

$$-\varepsilon_r E_P + \varepsilon_{\text{air}} E_A = \frac{\sigma_e}{\varepsilon_0} \tag{1}$$

$$d \cdot E_P + d_A \cdot E_A = 0 \tag{2}$$

where ε_r and E_P represent the relative permittivity and the electric field of the FEP electret layer, respectively, ε_{air} and E_A denote relative permittivity and electric field intensity of the air layer, respectively, σ_e is the surface charge density of the electret film, ε_0 is the permittivity of vacuum and d and d_A are the thicknesses of the electret layer and air layer, respectively.

Thus, the electric field in the air gap is given by

$$E_A = \frac{\sigma_e d}{\varepsilon_0(\varepsilon_r d_A + d)} \tag{3}$$

and the induced charge density σ_B on the bottom (or counter) electrode is given by

$$\sigma_B = -\varepsilon_0 E_A = -\frac{\sigma_e d}{\varepsilon_r d_A + d} \tag{4}$$

Since the device can be equivalent to an electret capacitor and an air capacitor in series, its capacitance is given by

$$C = \frac{\varepsilon_0 \varepsilon_r S}{\varepsilon_r d_A + d} \tag{5}$$

where S is the effective area of the bottom electrode

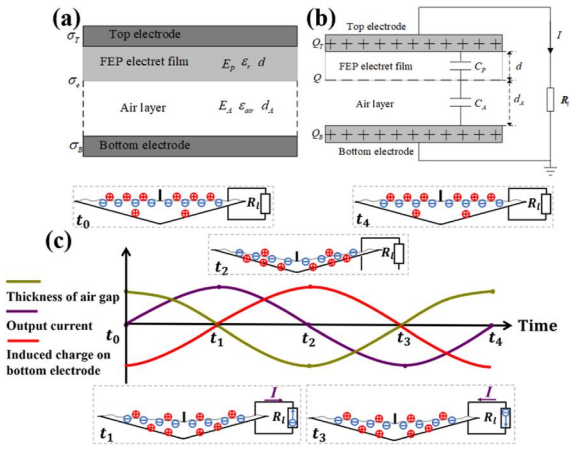

FIGURE 2 Working mechanism of the vibrational energy harvester. (a) The simplified model of electric field and charge distribution. (b) The simplified model of the device capacitance. (c) A schematic diagram of the working principle of the resilient electret film-based vibrational energy harvester. For a short circuit condition, sinusoidal variations of the air gap thickness cause the illustrated changes of the induced charge on the top and bottom electrodes and final output current. Note: For finite values of R_l, there will be an additional phase shift between these quantities (not shown in Figure 2c).

As shown in Figure 2c, during the vibration, the reduction of air gap thickness drives the current flow through the load resistor and leads to more induced positive charges accumulating on the bottom electrode. Conversely, as the air gap becomes larger, the current direction will be reversed. Therefore, the resilient FEP electret film functions effectively as an electron pump that drives electrons back and forth between the two electrodes.

3 | FINITE ELEMENT SIMULATION

3.1 | Finite element model

As analyzed above, the variation of the thickness of the air gap is one of the key factors influencing the energy conversion for the energy harvester. Therefore, the finite element (FE) software ABAQUS, which is suitable for structural dynamic response analysis was adopted in this study to simulate the fluctuation of the thickness of the air gap in the structure. The model for FE analysis (Figure 3) was established based on the structure of the energy harvester (Figure 1). Due to the lower stiffness of the wave-shaped FEP electret film, large deformation occurs during the vibration process of the energy harvester. In order to ensure the calculation accuracy, the film was divided into a 5-layer mesh in the thickness direction, and the aspect ratio of each element is 1:1 (Figure 3). The element (four-node bilinear plane strain quadrilateral element and reduced integral) in ABAQUS software was selected as the element in the FE model, and the total number of the elements is 49744 in the presently studied device. In the FE model, the FEP electret film, V-shape frame and seismic mass are isotropic materials, and their respective material properties, including density, Young's modulus and Poisson's ratio are listed in Table 1. According to the structural characteristics of the energy harvester, the wave-shaped FEP electret film, the V-shaped frame and the seismic mass were bonded together at the contact parts in the FE model. The acceleration, which satisfies the function $a_y = a\cos\omega t$ was applied to the bottom of the V-shaped frame to imitate the vibration of the device.

3.2 | Resonant frequency, initial deformation and dynamic response

The seismic mass was placed at the center of the wave-shaped FEP electret film in the device which introduces an initial

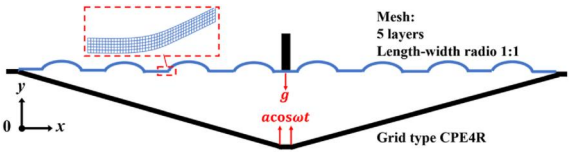

FIGURE 3 The finite element (FE) simulation model and mesh configuration for the vibrational energy harvester. The thickness between the two center points (the bottom of the seismic mass and the bottom of the V-shaped counter electrode) is the largest.

deformation of the film. Therefore, the structural deformation under the action of gravity was calculated by quasi-static analysis in ABAQUS software first. Taking into account of the deformation of the FEP film under the gravity of the seismic mass, the bending stiffness of the FEP film in the device can be obtained, which will be used to determine the resonant frequency of the harvester [34, 35], as will be discussed in the next section. In this quasi-static calculation, the displacement of the bottom of the V-shaped frame is directly fixed, that is, $u_y = 0$.

For the energy harvesters with the mounted wave-shaped FEP films showing a pre-stretched state, the simulation of the stretching of the film was carried out first and then the deformation of the film under the action of gravity was calculated.

The resonant frequency analysis of the energy harvester was directly carried out in the 'Frequency' analysis mode in the ABAQUS software where the resonant frequencies and corresponding modes were obtained from the 'Eigenvalue output'.

In order to simulate the dynamic response of the wave-shaped FEP electret film during the vibration, a cosine acceleration load (Figure 3) was exerted on the V-shaped electrode in the vertical direction (*y*-axis) to drive the motion of the shaker, and the 'Steady-state dynamics' analysis mode in the ABAQUS was adopted to simulate the dynamic response of the energy harvester. Here, large deformation analysis was utilized. The dynamic response of each node was extracted from the result files and visualized.

3.3 | Output power

In order to collect the data of the air gap thickness, 33 nodes on the bottom edge of the electret film and seven nodes on the V-shaped counter electrode were selected as feature nodes to characterise the structural deformation in the simulation (Figure 4). Since the maximum frequency of vibration was 100 Hz in the study, the coordinate information of the feature nodes was extracted every 1 ms from the ABAQUS result files. By connecting adjacent feature points with line segments and fitting a linear function, the segment function of 32 segments is sufficient to characterize the shape and position of the electret film. Similarly, the position and shape of the V-shaped electrode can also be characterised by the coordinate data of the characteristic node at each time step.

Since the conductor surface is equipotential and the electric field lines are perpendicular to the surface, the air gap thickness at any time corresponding to any position of the structure is easily calculated as shown by $d_{A(x,t)}$ in Figure 4. Substituting it into Equation (5) and performing the integration operation, the total capacitance of the energy harvester at time t can be obtained as

$$C(t) = 2 \times \int_0^{L/2} \frac{\varepsilon_0 \varepsilon_r W \sqrt{1+k^2}}{\varepsilon_r d_A(x,t) + d} \mathrm{d}x \tag{6}$$

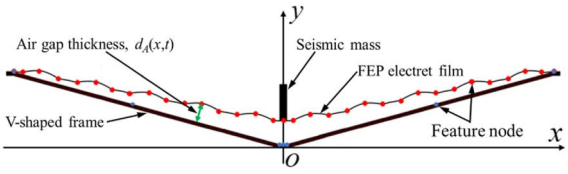

FIGURE 4 Schematic diagram of feature nodes and air gap thickness of the harvester. The arrow in green shows the thickness of the air gap between a node on the FEP film and the counter electrode.

Similarly, substituting d_A (x,t) into Equation (4) and integrating, the amount of induced charge on the bottom electrode at time t is given by

$$Q_B(t) = 2 \times \int_0^{L/2} -\frac{\sigma_e W d \sqrt{1+k^2}}{\varepsilon_r d_A(x,t) + d} \mathrm{d}x \tag{7}$$

where L and W are the length and width of the electret film, respectively, and ε_0 is the permittivity of vacuum, ε_r is the relative permittivity of the FEP electret film, d is the thickness of the electret layer, k is the slope of the V-shaped counter electrode and σ_e is the surface charge density of the electret film.

The output current of the energy harvester can be obtained by differentiating the amount of induced charge on the bottom electrode with respect to time as

$$I(t) = \frac{\mathrm{d}Q_B(t)}{\mathrm{d}t} \tag{8}$$

The matching load resistance is given by [31].

$$R_{\mathrm{opt}} = \frac{1}{\omega_0 C} \tag{9}$$

where ω_0 and C are the angular resonant frequency and the initial capacitance of the device, respectively.

Then the output power of the energy harvester with a matching resistance is calculated by

$$P_{\mathrm{out}} = \frac{\int_{t_1}^{t_2} I^2(t) R_{\mathrm{opt}} \mathrm{d}t}{t_2 - t_1} \tag{10}$$

And finally, the normalized output power of the energy harvester is given by

$$P_n = P_{\mathrm{out}} \left(\frac{g}{a}\right)^2 \tag{11}$$

where t_1, t_2 are the start and end time of vibration, respectively, g is the gravitational acceleration and a is the actual acceleration of the vibration.

4 | EXPERIMENTAL WORK

The preparation of the highly elastic FEP electret film includes a template-based hot-pressing process to form a wavy structure and a polarisation process to deposit negative charges on it

[19, 20, 31, 36]. Figure 5a presents the optical image of a prepared resilient FEP electret film. Before polarization, an aluminium electrode with a thickness of 100 nm was first deposited on the upper surface of the wave-shaped FEP film by vacuum evaporation. Afterwards, the other side of the film was exposed to a grid-controlled corona charging setup. The grid voltage, corona needle voltage and charging time are −1 kV, −10 kV and 5 min, respectively. After polarization treatment, the negative charge density of the bottom surface of the FEP electret film was finally stabilized at about 0.42 mC/m^2. Both ends of the negatively charged wave-shaped FEP electret film were pasted on the copper V-shaped counter electrode, and a seismic mass was attached to the center of the upper surface of the film [Figure 5b] to assemble the energy harvester. The current harvester configuration can avoid discharge during vibration, owing to the fact that the surface charge density of the wave-shaped FEP film is well controlled by the Paschen law which guarantees that no Paschen breakdown happens in the air gap during vibration. In addition, a very small portion of the whole area of the FEP film can touch the bottom V-shaped counter electrode even in case of an accident because of its wavy-shaped structure. Thus, even in such a case most of the charges will remain in the FEP films [31].

For the output power measurement, the bottom of the energy harvester is fixed on the electrodynamic shaker (B&K 4809). The signal generated by an audio analyzer (Digital Audio Analyzer dScope series III) was first amplified with a power amplifier (B&K 2713) and then connected with the shaker to excite its vibration. At the same time, the charge generated by the energy harvester was amplified with a charge amplifier (B&K 2635) and then recorded by the audio analyzer. The acceleration was measured by an accelerometer (B&K 4393), as shown in Figure 5d.

Ignoring the mass of the FEP electret film, the angular resonant frequency ω_0 of the harvester is theoretically determined by [19]

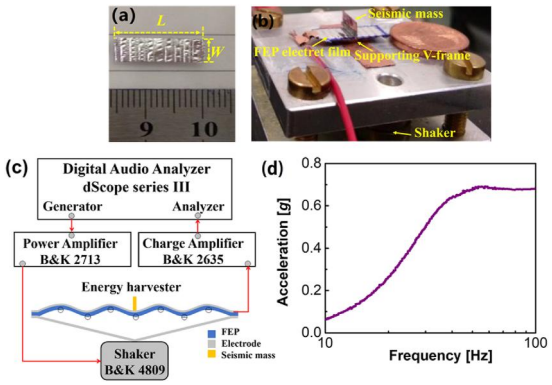

FIGURE 5 (a) An optical image of the wave-shaped resilient FEP electret film sample (length L = 15 mm, width W = 5 mm and thickness d = 0.0125 mm), (b) An optical image of the vibrational energy harvester mounted on a shaker, (c) The experimental setup for measuring output power of the harvester and (d) the measured acceleration of the shaker as a function of excitation frequency from 10 to 100 Hz.

$$\omega_0 = \sqrt{\frac{k_m}{m_s}} \tag{12}$$

where k_m is the elastic modulus of the electret film, and m_s is the seismic mass. The output power at a matching load resistance is given by the following equation [31], that is,

$$P_{\text{out}} = \frac{1}{2} R_{\text{opt}} \omega^2 Q_{\text{rms}}^2 \tag{13}$$

where ω is the angular frequency of the vibration and Q_{rms} is the RMS value of the generated charge in short circuit and R_{opt} is the matching resistance. The output power reported in this study is calculated with Equation (13), where the charge Q is measured in short circuit, and the optimal resistance R_{opt} is obtained with Equation (9) using the measured resonant frequency and capacitance of the device.

Finally, the output power of the energy harvester obtained experimentally was also normalized by Equation (11).

5 | RESULTS AND DISCUSSION

5.1 | Resonant frequency

The resonant frequency is one of the crucial factors that influences the efficiency of an energy harvester because normally the maximum power output is obtained at it. Therefore, the influence of the initial stretching state of the wave-shaped FEP electret film and the seismic mass on the resonant frequency of the device were investigated with the FE simulation method first.

The dimensions of the FE model in this study are 15 × 5 × 2 mm^3, where the length and width of the wave-shaped FEP film are 15 and 5 mm, respectively, and the height of the device is 2 mm. The thickness of the FEP and the seismic mass are 12.5 μm and 25 mg, respectively.

The resonant frequencies of the device under various conditions were obtained by harmonic response analysis in a software package ABAQUS. These data are also the basis for the subsequent dynamic simulation and calculation of the power output. Since the stiffness of the wave-shaped FEP film in the device is not only affected by its material properties and geometry but also by the tension which is caused by the initial stretching state of the FEP film fixed on the V-shaped frame. Simulation results of the pre-stretching state of the wave-shaped FEP electret film on resonant frequency of the device are shown in Figure 6a. Also shown are the corresponding initial thickness values $d_{A(0,0)}$ of the air gap at the axis of symmetry because they are associated with the capacitance of the variable capacitor, and, thus, affect the output power of the device. As indicated in Figure 6a, a larger stretching length results in a larger initial air gap thickness, which is caused by the enhancement of stiffness of the wave-shaped FEP film in the stretched state. The resonant frequency is about 29.4 Hz, and the initial air gap thickness is 1.11 mm, when there is no initial tension on the electret film. Increasing the stretching

length of the wave-shaped FEP film by 0.06 mm with an initial length of 15 mm, corresponding to a strain of 0.4%, the resonant frequency slightly decreases to 27.3 Hz. However, when the stretching length exceeds 0.06 mm, the resonant frequency significantly increases up to 70 Hz at a stretching length of 0.24 mm, corresponding to a strain of 1.6%. However, the thickness of the air gap always increases with the stretching length as expected. Thus, the resonant frequency can be tuned in a relatively broad range from 29.4 to 70 Hz, which makes the device more flexible for adapting to various vibrational frequencies in the environment.

Seismic mass is another factor influencing the resonant frequency as expected from Equation (12). Simulation results on the influence of seismic mass on the resonant frequency [Figure 6b] indicate that resonant frequency increases with increasing seismic mass as expected, that is, ranging from 67.6 to 38.8 Hz as the seismic mass increases from 25 mg to 0.1 g when keeping a constant stretching length of 0.24 mm. In addition, the initial air gap thickness at the axis of symmetry decreases from 1.94 to 1.76 mm, accordingly.

5.2 | Dynamic response

Figure 7 presents the simulation results on the dynamic responses of the energy harvester to an external vibration with a frequency of 24 Hz and an acceleration of 0.172 g, including the thickness of the air gap, capacitance, the induced charge on bottom electrode and the current in short circuit. The initial stretching length of the wave-shaped FEP electret film is 0.08 mm. Since the acceleration excitation is directly applied to the bottom of the V-shaped frame which has a much larger stiffness comparing with the wave-shaped FEP film, the dynamic response displacement of the V-shaped frame and that of the wave-shaped FEP film fixed with a seismic mass is not synchronous. Therefore, the thickness of the air gap between the FEP film and the frame is a superposition of their relative displacement, where a similar beat phenomenon appears. Figure 7a depicts that the thickness of the air layer varies in the range from 1.06 to 2.14 mm at the axis of symmetry during the vibration. Comparing Figure 7b,c and a, it reveals that both the capacitance of the device and the induced charge on the bottom electrode increase with reducing the air gap thickness, and, thus, the current flows from the top electrode to the bottom electrode. Conversely, the direction of the current flows in an opposite direction as the air gap thickness becomes larger. As expected, the current is proportional to the variation rate of the induced charge on the electrode [Figure 7d]. The energy of capacitors is a function of state in the thermodynamic sense, and, thus, it depends only on the electrical and mechanical state of the capacitor and not on the history of the device.

The comparison of the current of the energy harvester at the vibration frequencies of 24, 28 and 32 Hz [Figure 8a] indicates that the frequency of the current generated is always the same as that of the driving vibrational frequency, and the current generated at the resonant frequency of 28 Hz is significantly larger than those in the other two cases. This is reasonable because the maximum variation of the air gap thickness always happens at the resonant frequency [Figure 8b], which results in the maximum current and output power. Therefore, for the presently studied energy harvester, the most efficient energy harvesting is at its resonant frequency of about 28 Hz, which is also consistent with the results of the harmonic response analysis.

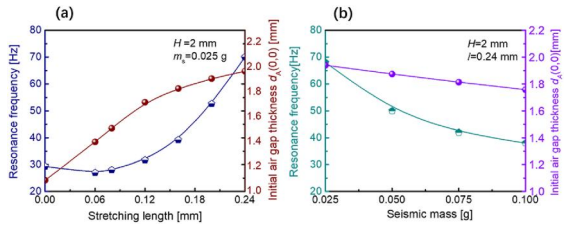

FIGURE 6 Simulated resonance frequency and initial air gap thickness of the harvester (a) at different stretching lengths of the resilient FEP film and (b) loaded with different seismic masses.

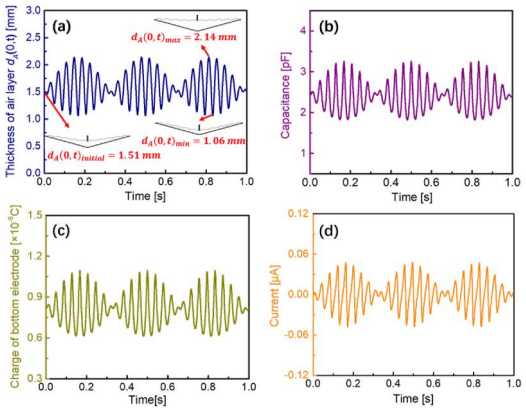

FIGURE 7 Simulation of dynamic response of the vibrational harvester with parameters of $H = 2$ mm, $l = 0.08$ mm, $f = 24$ Hz and $m_s = 25$ mg. (a) Air layer thickness at the axis of symmetry versus time. (b) Device capacitance versus time. (c) Transferred induced charge of the bottom electrode versus time. (d) Output current versus time.

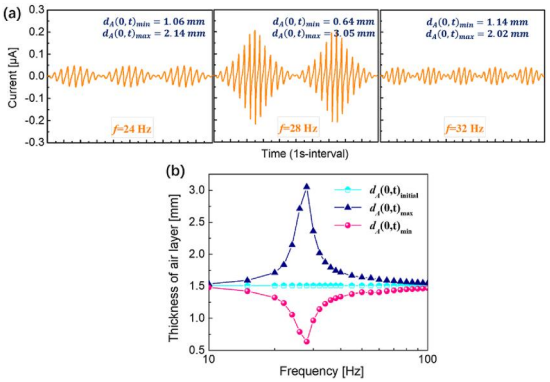

FIGURE 8 Comparison of dynamic response under different excitation frequencies with harvester parameters of $H = 2$ mm, $l = 0.08$ mm and $m_s = 25$ mg, (a) Comparison of output current in one second with an excitation frequency of 24 Hz, 28 and 32 Hz. (b) Initial, maximum and minimum air gap thickness versus excitation frequency.

5.3 | Power output

The frequency dependence of the power output of the energy harvesters constructed according to the above described devices was investigated by FE simulation and verified by experiments. These energy harvesters have a size of 15 × 5 × 2 mm^3 and a seismic mass of 25 mg. The relationships between the normalised output power and the vibrational frequency, obtained by FE simulation, are illustrated in Figure 9a with the pre-stretching length as a parameter. The results show that the maximum power output is always obtained at the resonant frequency of the device for all initial stretching states. The resonant frequency shifts from 28 to 68 Hz as the initial stretching length varies from 0.08 to 0.24 mm, corresponding to a strain of 0.5%–1.6%. For the samples with an initial stretching length of 0.08 mm, the simulation results show that the normalized output power reaches 233 μW at its resonant frequency of 28 Hz. However, with the increasing initial stretching length, the normalized output power at the resonant frequency decreases. For the sample with an initial stretching length of 0.24 mm, the maximum output power is only 9 μW at its resonant frequency of 68 Hz. Figure 9b shows the experimentally obtained output power versus excitation frequency at various stretching lengths of the wave-shaped FEP electret film. The corresponding acceleration used in the experiments is presented in Figure 5d. The normalized values of the output power obtained experimentally are illustrated in Figure 9c. In order to make the comparison easier, both the simulation results and experimental data are depicted in Figure 9c, showing good agreement. In order to compare the simulation results and the experimental data directly, the dependence of maximum output power and resonant frequency on the stretching length is plotted in Figure 9d , where the experimental data are averaged over five samples. Obviously, the experimental data agrees well with the simulation results. In addition, the results are also consistent with the theoretical results obtained by harmonic response analysis. As a result, the resonant frequency of the energy harvester can be tuned effectively in a broad frequency range by merely adjusting the initial stretching state of the wave-shaped FEP electret film, allowing for a better adaptability to complex environmental vibration sources. However, the corresponding output power at the resonant frequency decreases with increasing resonant frequency for an otherwise constant seismic mass. The increase of the resonant frequency is due to the increasing stiffness of the wave-shaped FEP electret film with an increasing initial stretching length, which reduces its deformability during vibration.

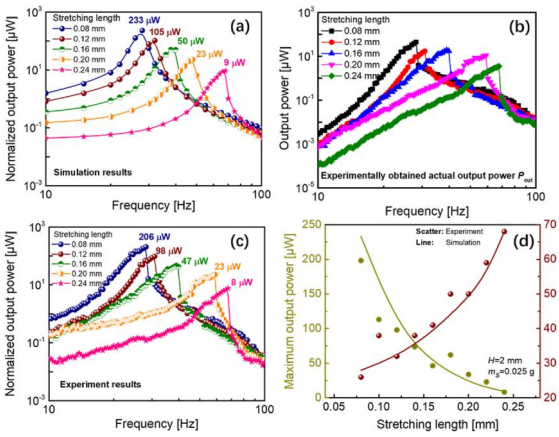

FIGURE 9 Influence of pre-stretching of the resilient electret on resonance frequency and output power of the harvester with parameters of $H = 2$ mm and $m_s = 25$ mg, (a) Simulated normalised output power versus excitation frequency with different stretching lengths of the resilient FEP electret film. (b) Experimentally obtained actual output power versus excitation frequency for different stretching lengths of the resilient FEP electret film. (c) Experimentally obtained normalised output power based on the results is shown in Figure 9b. (d) Comparison of simulated and experimental results of the effect of the resilient electret pre-stretched state on maximum output power and resonance frequency.

Seismic mass is another important factor that influences both the resonant frequency as expressed in Equation (12) and the output power as discussed in the following. Regarding the presently studied electret-based energy harvester as a 'black box", its output power can be adapted from the piezoelectret energy harvester as follows [37]:

$$P_{\text{out}} = \frac{{m_s}^2 d_{eff}^2 a^2 R_l \omega^2}{\left[\left(\omega^2/{\omega_0}^2 - 1\right)^2 + 4{\zeta_m}^2(\omega/\omega_0)^2\right]\left[1 + (R_l/R_c)^2\right]} \tag{14}$$

where m_s is the seismic mass, d_{eff} is the effective piezoelectric coefficient, a is the amplitude of acceleration excitation, R_l is the load resistance, ω is the angular frequency of acceleration, ω_0 is the angular resonant frequency, ζ_m is the mechanical damping ratio and R_c is the capacitive resistance of the harvester.

The maximum output power delivered to the load resistor with a matching resistance $R_l = R_c = 1/(\omega_0 C)$ at the resonant frequency is given by the following equation [36]

$$P_m = \frac{{m_s}^2 d_{eff}^2 a^2 \omega_0}{8{\zeta_m}^2 C} \tag{15}$$

Therefore, considering the relation between the resonant frequency and the seismic mass in Equation (12), we can conclude that the maximum output power at the resonant frequency is proportional to $m_s^{-3/2}$. Keeping the initial stretching length of the wave-shaped FEP electret film at 0.24 mm, the simulation results shown in Figure 10a indicate that the resonant frequency of the device shifts from 68 to 38 Hz with increasing seismic mass from 25 mg to 0.1 g. The maximum output power at the resonant frequency thereby significantly increases from 9 to 40 μW. The experimental data shown in Figure 10b are in good agreement with the simulation results in Figure 10a. From Figure 10a and Figure 10b one can also observe the abrupt drop of the output power above the resonant frequency. This is assumed to be due to the non-linearity of the deformation of the wave-shaped FEP film caused by its geometric non-linearity. An intuitive and full

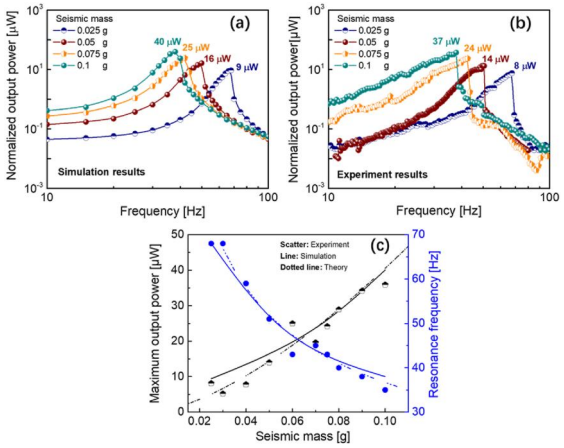

FIGURE 10 Effect of seismic mass on resonance frequency and output power with harvester parameters of $H = 2$ mm and $l = 0.24$ mm. (a) Simulated normalized output power versus frequency for different seismic masses. (b) Experimentally obtained normalized output power versus frequency with different seismic masses. (c) Comparison of simulation, experimental and theoretical analysis results of the effect of the seismic mass on maximum output power and resonance frequency.

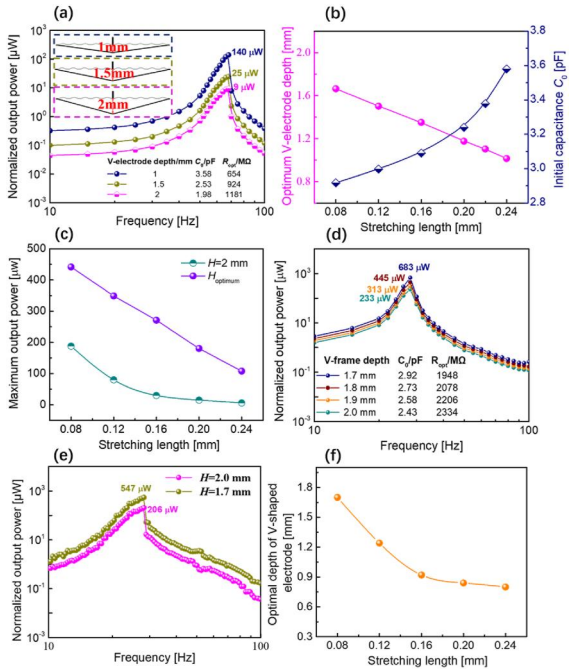

FIGURE 11 Effect of the depth of the V-shaped counter electrode on the energy harvesting performance. (a) Simulated normalized output power of harvesters with depths of 1, 1.5 and 2 mm, respectively. (b) Improved depth of the V-shaped counter electrode and initial capacitance of the optimized harvester device versus the stretching length of the resilient electret film. (c) Comparison between the original device and optimized device in terms of the maximum output power with various stretching lengths of the resilient electret film. (d) Effect of the depth of the V-shaped electrode on the output power of the energy harvester. (e) Experimentally normalized output power versus frequency for harvesters with various depths of the V-shaped counter electrode. (f) Dependence of optimized depth of the counter electrode on initial stretching length of the resilient FEP film.

comparison of the theoretical predictions, the simulation results extracted from Figure 10a and the experimental data which is an average of five samples are illustrated in Figure 10c. This figure indicates that the theoretical predictions, the simulation results and the experimental results are consistent and in fair agreement.

Since the energy stored in the variable capacitor of the energy harvester is determined by the structure of the device and the electret film providing the embedded biased voltage, the V-shape of the counter electrode is a crucial parameter for optimizing the efficiency of the energy harvester since it influences the capacitance of the device significantly during vibration. For an energy harvester with given parameters for the size of the wave-shaped FEP electret film, the initial stretching length (or strain) and seismic mass, the variation of the capacitance is determined by the maximum capacitance that the device can achieve during vibration. The counter electrode with a V shape as designed in this study allows the device to achieve a large capacitance when the electret film is very close to the counter electrode during vibration. Therefore, the effect of the depth H of the V-shaped electrode was studied and the results are shown in Figure 11.

First of all, the change of depth of the V-shaped electrode has no influence on the resonant frequency of the device because it hardly deforms during the vibration process and can be regarded as a rigid body. When the depth of the V-shaped electrode is gradually reduced, the output power of the energy harvester increases significantly as shown in Figure 11a. This figure depicts that for a device sample with an initial stretching length of 0.24 mm and a seismic mass of 25 mg, the normalized output power at the resonant frequency is only 9 μW for the device with a V-shaped electrode depth of 2 mm. Nevertheless, the output power increases to 25 μW when the depth decreases to 1.5 mm and dramatically enhances to 140 μW when the depth further reduces to 1 mm. It is worth noting that the contact between the electret film and the V-shaped electrode throughout the whole vibration process should be avoided for preventing the detrapping of surface charge stored in the resilient FEP electret film. Therefore, it is important to obtain the adjustable range of the depth of the V-shaped electrode so that the energy harvesting efficiency can be effectively improved on the basis of the normal operation of the device. The pink line in Figure 11b shows the improved depth of the V-shaped bottom electrode corresponding to different initial stretching states of the electret film with a seismic mass of 25 mg. With the increase of the initial stretching length of the electret film from 0.08 to 0.24 mm, the improved depth of the V-shaped electrode decreases almost linearly from 1.66 to 1.01 mm. Two main reasons can account for this phenomenon. First, the electret film with a larger pretension is more difficult to deform under the same seismic mass and acceleration. Second, the enhancement in the tensile stiffness and bending stiffness of the electret film is due to pre-stretching limits and its large deformation during vibration. And the initial capacitance of the device will be greatly improved if

TABLE 2 Comparison of our work with reported electret-based energy harvesters

Year [Ref.]	Device size	Seismic mass [g]	Resonant frequency [Hz]	Acceleration [*g*]	Output power [μW]
2018 [27]	295.8 mm^3	0.0913	736	1.3	14.8
2018 [31]	4 cm^2	80	90	1	1850
2019 [36]	3 cm^2	3	22	1	355
2020 [28]	252.3 cm^3	/	/	/	691
2021 [25]	234 mm^2	/	154	2.9	11.72
2021 [19]	2100 mm^3	0.08	20	1	261
This work	127.5 mm^3	0.025	28	1	547

the corresponding optimal V-shaped electrode depth is adopted, especially for the ones with large pre-stretching length, as shown by the blue curve in Figure 11b.

Figure 11c illustrates the comparison between the maximum output power of the device before and after the optimization of the depth of the V-shaped counter electrode. This figure indicates that the output power is significantly improved after optimization of the structure of the device. As depicted in Figure 11d, the normalized output power at the resonance frequency is 233 μW at an initial stretching length of 0.08 mm. However, when reducing the depth of the V-shaped counter electrode to the optimized value of 1.7 mm, the maximum output power increases to 683 μW, almost three times the initial output power. For a device with a depth of 1.7 mm for the V-shaped counter electrode, the maximum voltage output in an open circuit can reach up to 531 V. These simulation results were also verified by the experimental data. As shown in Figure 11e, the output power of the energy harvester is enhanced from 206 to 547 μW due to the optimization of the depth of the V-shaped counter electrode. Figure 11f depicts the relation between the optimal depth of the V-shaped counter electrode and the initial stretching length. It can be noted that the optimal depth of the V-shaped counter electrode decreases from 1.7 to 0.8 mm as the initial stretching length increases from 0.08 to 0.24 mm.

Table 2 compares our work with other reported electret-based energy harvesters in terms of device size, seismic mass, resonant frequency, acceleration and output power [19, 25, 27, 28, 31, 36]. It appears that the introduced vibrational energy harvester in this work adds to the list of attributes including miniature device and high output power, which enable new possibilities in this field.

6 | CONCLUSION

In this study, a vibrational energy harvester, consisting of a negatively charged high resilient FEP electret film, a seismic mass and a V-shaped counter electrode, was designed and optimized with the FE simulation. The reliability of the FE model and the correctness of the simulation results were verified by experiments. The resonant frequency of the energy harvester can be tuned by simple adjustment of the initial stretching state of the wave-shaped FEP film and the seismic mass in a broad frequency range. The output power of the device can be optimized by controlling the depth of the V-shaped counter electrode. For an optimized vibrational energy harvester sample with a volume of 15 × 5 × 1.7 mm^3 and a seismic mass of 25 mg, the maximum normalized output power obtained experimentally is 547 μW at its resonant frequency of 28 Hz, corresponding to a volume power density of 4.3 $\mu W/mm^3$, which is efficient to power some low-power-assumption electronics.

AUTHOR CONTRIBUTIONS

Xiaoya Yang and **Xingchen Ma** contributed equally. **Xiaoya Yang:** Methodology; Investigation; Writing-original draft; Data curation. **Xingchen Ma:** Methodology; Writing – review; Validation; Formal analysis. **Chuan Ding:** Methodology. Data curation. **Gerhard M. Sessler:** Formal analysis. Validation. **Heinz von Seggern:** Formal analysis, Validation. **Mario Kupnik:** Formal analysis, Validation. **Ying Dai:** Review & editing. **Pengfei He:** Review & editing. **Xiaoqing Zhang:** Conceptualization, Formal analysis, Review & editing, Project administration.

ACKNOWLEDGEMENTS

Financial support from the Natural Science Foundation of China (NSFC, Grant Nos. 61761136004 and 62201392), Shanghai Post-doctoral Excellence Program (Grant No. 2021341), and the Deutsche Forschungsgemeinschaft (DFG, German Research Foundation, KU 3498/1-1, SE 941/19-1, SE 941/21-1) is gratefully acknowledged.

CONFLICT OF INTEREST

The authors declare no conflict of interest.

DATA AVAILABILITY STATEMENT

The data that support the findings of this study are available from the corresponding author upon reasonable request.

REFERENCES

1. Sengupta, A., et al.: Flexible nanogenerator from electrospun PVDF–polycarbazole nanofiber membranes for human motion energy-harvesting device applications', ACS biomater. Sci. Eng. 7(4), 1673–1685 (2021). https://doi.org/10.1021/acsbiomaterials.0c01730
2. Fang, S., et al.: Analytical and experimental investigation of the centrifugal softening and stiffening effects in rotational energy harvesting. J. Sound Vib. 488, 115643 (2020). https://doi.org/10.1016/j.jsv.2020.115643

3. Sahu, M., et al.: Development of triboelectric nanogenerator and mechanical energy harvesting using argon ion-implanted kapton, zinc oxide and kapton. Mater. Lett. 301, 130290 (2021). https://doi.org/10.1016/j.matlet.2021.130290
4. Zhang, L.B., et al.: Design of high-efficiency electromagnetic energy harvester based on a rolling magnet. Energy Convers. Manag. 185, 202–210 (2019). https://doi.org/10.1016/j.enconman.2019.01.089
5. Shan, X., et al.: Enhancing the performance of an underwater piezoelectric energy harvester based on flow-induced vibration. Energy 172, 134–140 (2019). https://doi.org/10.1016/j.energy.2019.01.120
6. Rajarathinam, M., Ali, S.F.: Energy generation in a hybrid harvester under harmonic excitation. Energy Convers. Manag. 155, 10–19 (2018). https://doi.org/10.1016/j.enconman.2017.10.054
7. Diankun, P., Fuhong, D.: Design and analysis of a broadband vibratory energy harvester using bi-stable piezoelectric composite laminate. Energy Convers. Manag. 169, 149–160 (2018). https://doi.org/10.1016/j.enconman.2018.05.032
8. Paul, S., Chang, J.: Design of novel electromagnetic energy harvester to power a deicing robot and monitoring sensors for transmission lines. Energy Convers. Manag. 197, 111868 (2019). https://doi.org/10.1016/j.enconman.2019.111868
9. Salauddin, M., et al.: Design and experiment of hybridized electromagnetic-triboelectric energy harvester using Halbach magnet array from handshaking vibration. Energy Convers. Manag. 153, 1–11 (2017). https://doi.org/10.1016/j.enconman.2017.09.057
10. Deng, W., Wang, Y.: Systematic parameter study of a nonlinear electromagnetic energy harvester with matched magnetic orientation: numerical simulation and experimental investigation. Mech. Syst. Signal Process. 85, 591–600 (2017). https://doi.org/10.1016/j.ymssp.2016.09.002
11. Li, W., et al.: Flexible and biocompatible polypropylene ferroelectret nanogenerator (FENG): on the path toward wearable devices powered by human motion. Nano Energy 30, 649–657 (2016). https://doi.org/10.1016/j.nanoen.2016.10.007
12. Zhang, X., et al.: Ferroelectret nanogenerator with large transverse piezoelectric activity. Nano Energy 50, 52–61 (2018). https://doi.org/10.1016/j.nanoen.2018.05.016
13. Hu, Y., Wang, Z.: Recent progress in piezoelectric nanogenerators as a sustainable power source in self-powered systems and active sensors. Nano Energy 14, 3–14 (2015). https://doi.org/10.1016/j.nanoen.2014.11.038
14. Khan, F.U., Ahmad, S.: Flow type electromagnetic based energy harvester for pipeline health monitoring system. Energy Convers. Manag. 200, 112089 (2019). https://doi.org/10.1016/j.enconman.2019.112089
15. Lu, Y., et al.: The PZT/Ni unimorph magnetoelectric energy harvester for wireless sensing applications. Energy Convers. Manag. 200, 112084 (2019). https://doi.org/10.1016/j.enconman.2019.112084
16. Zhong, J., et al.: Flexible PET/EVA-based piezoelectret generator for energy harvesting in harsh environments. Nano Energy 37, 268–274 (2017). https://doi.org/10.1016/j.nanoen.2017.05.034
17. Wu, N., et al.: Output enhanced compact multilayer flexible nanogenerator for self-powered wireless remote system. J. Mater. Chem. 5(25), 12787–12792 (2017). https://doi.org/10.1039/c7ta03574h
18. Wang, B., et al.: Sandwiched composite fluorocarbon film for flexible electret generator. Adv. Electron. Mater. 2(4), 1500408 (2016). https://doi.org/10.1002/aelm.201500408
19. Ma, X., et al.: Theoretical analysis and experimental validation of frequency-moldable electrostatic energy harvesters biased with a high elastic electret film. Smart Mater. Struct. 30(6), 065021 (2021). https://doi.org/10.1088/1361-665x/abfb83
20. Ma, X., et al.: Tuneable resonance frequency vibrational energy harvester with electret-embedded variable capacitor. IET Nanodielectrics 4(2), 1–10 (2021). https://doi.org/10.1049/nde2.12007
21. Sakane, Y., Suzuki, Y., Kasagi, N.: Development of high-performance perfluorinated polymer electret for micro seismic power generation. In: The Proceedings of the National Symposium on Power and Energy Systems 13(0), 429–430 (2008). https://doi.org/10.1299/jsmepes.2008.13.429
22. Madinei, H., et al.: Adaptive tuned piezoelectric MEMS vibration energy harvester using an electrostatic device. Eur. Phys. J. Spec. Top. 224(14-15), 2703–2717 (2015). https://doi.org/10.1140/epjst/e2015-02584-6
23. Oxaal, J., et al.: Investigation of gap-closing interdigitated capacitors for electrostatic vibration energy harvesting. J. Micromech. Microeng. 25(10), 105010 (2015). https://doi.org/10.1088/0960-1317/25/10/105010
24. Li, M., et al.: Recent progress on mechanical optimization of MEMS electret-based electrostatic vibration energy harvesters. J. Microelectromech. Syst. 31(5), 726–740 (2022). https://doi.org/10.1109/jmems.2022.3194859
25. Luo, A., et al.: Spray-coated electret materials with enhanced stability in a harsh environment for an MEMS energy harvesting device. Microsyst. Nanoeng. 7(1), 15 (2021). https://doi.org/10.1038/s41378-021-00239-0
26. Luo, A., et al.: Optimization of MEMS vibration energy harvester with perforated electrode. J. Microelectromech. Syst. 30(2), 299–308 (2021). https://doi.org/10.1109/jmems.2021.3058766
27. Tao, K., et al.: Investigation of multimodal electret-based MEMS energy harvester with impact-induced nonlinearity. J. Microelectromech. Syst. 27(2), 276–288 (2018). https://doi.org/10.1109/jmems.2018.2792686
28. Tao, K., et al.: Miura-origami-inspired electret/triboelectric power generator for wearable energy harvesting with water-proof capability. Microsyst. Nanoeng. 6(1), 56 (2020). https://doi.org/10.1038/s41378-020-0163-1
29. Zhang, X., et al.: Fluoroethylenepropylene ferroelectrets with patterned microstructure and high, thermally stable piezoelectricity. Appl. Phys. 107(3), 621–629 (2012). https://doi.org/10.1007/s00339-012-6840-7
30. Zhang, X., et al.: Fabrication of fluoropolymer piezoelectrets by using rigid template: structure and thermal stability. J. Appl. Phys. 108(6), 064113 (2010). https://doi.org/10.1063/1.3482011
31. Zhang, X., et al.: Broad bandwidth vibration energy harvester based on thermally stable wavy fluorinated ethylene propylene electret films with negative charges. J. Micromech. Microeng. 28(6), 065012 (2018). https://doi.org/10.1088/1361-6439/aab57d
32. Emmerich, F., Thielemann, C.: Optimizing dimensions of unipolar Teflon-FEP piezoelectrets with micro-system-technology. J. Phys. Conf. 1052, 012052 (2018). https://doi.org/10.1088/1742-6596/1052/1/012052
33. Zhukov, S., et al.: Analytical prediction of the piezoelectric d33 response of fluoropolymer arrays with tubular air channels. Sci. Rep. 8(1), 4597 (2018). https://doi.org/10.1038/s41598-018-22918-1
34. Zhang, H., Ahmadi, M.: Resonance tuning of a multi-piezoelectric bimorph beams energy harvester connected by springs. Ferroelectrics 460(1), 34–48 (2014). https://doi.org/10.1080/00150193.2014.874898
35. Zhu, D., Tudor, M.J., Beeby, S.P.: Strategies for increasing the operating frequency range of vibration energy harvesters: a review. Meas. Sci. Technol. 21(2), 022001 (2010). https://doi.org/10.1088/0957-0233/21/2/022001
36. Ma, X., et al.: Energy harvesters based on fluorinated ethylene propylene unipolar ferroelectrets with negative charges. AIP Adv. 9(12), 125334 (2019). https://doi.org/10.1063/1.5086113
37. Hillenbrand, J., Pondrom, P., Sessler, G.M.: Electret transducer for vibration-based energy harvesting. Appl. Phys. Lett. 106(18), 183902 (2015). https://doi.org/10.1063/1.4919875

How to cite this article: Yang, X., et al.: Resilient electret film-based vibrational energy harvesters with a V-shaped counter electrode. IET Nanodielectr. 6(2), 36–45 (2023). https://doi.org/10.1049/nde2.12040